IEEE JOURNAL OF
PHOTOVOLTAICS
A PUBLICATION OF THE IEEE ELECTRON DEVICES SOCIETY, THE IEEE INDUSTRIAL ELECTRONICS SOCIETY, THE IEEE NANOTECHNOLOGY COUNCIL, THE IEEE PHOTONICS SOCIETY, THE IEEE POWER & ENERGY SOCIETY, THE IEEE POWER ELECTRONICS SOCIETY, AND THE IEEE RELIABILITY SOCIETY

Field-aged Glass/Backsheet and Glass/Glass PV Modules: Encapsulant Degradation Comparison

Aesha Patel, Archana Sinha, and Govindasamy Tamizhmani

***Abstract*— Ethylene vinyl acetate (EVA) is the predominant encapsulant in crystalline-silicon PV modules; however, its degradation is a subject of major concern, which causes significant power loss under field conditions. This paper presents a comparison of EVA degradation in field-aged PV modules with glass/backsheet (G/B) and glass/glass (G/G) architectures. Module-level characterization included UV Fluorescence imaging and *I-V* measurements. Material analytical techniques, including Colorimetry, Differential Scanning Calorimetry (DSC), Thermogravimetric Analysis (TGA), Fourier Transform Infrared Spectroscopy (FTIR), and Raman spectroscopy were performed to correlate the module performance parameters with EVA material properties. An intense EVA discoloration in G/G modules was observed which was corroborated by higher module I_{sc} and P_{max} degradation rates compared to its counterpart G/B modules. Higher power degradation was accompanied by a significant increase in EVA crosslinking, vinyl acetate content, yellowness index, and presence of functional groups containing unsaturated moieties that are linked to degradation products of photothermal reaction, and a higher decrease in degree of crystallinity The absence of a polymeric backsheet in hermetically sealed G/G modules which restricts photobleaching and enhances the entrapment of volatile acetic acid and other degradation by-products plays a major role in causing higher EVA degradation in G/G modules. This work concludes that EVA might have been a good choice of an encapsulant for the G/B modules over the decades, but it may prove to be an inappropriate choice for the G/G modules due to potential degassing, corrosion and/or discoloration issues. Ionomers or polyester-based encapsulants like polyolefins (POE) could be best suited for G/G modules as it appears to be a current trend in the industry.**

***Index Terms*—Characterization, crosslinking, degree of crystallinity, encapsulant degradation, ethylene vinyl acetate, field-aged, glass/backsheet, glass/glass, PV module**

I. Introduction

In recent years, solar photovoltaics (PV) has emerged as one of the most promising renewable energy sources. The worldwide deployment of PV modules has seen an exponential increase with diverse applications [1]. A PV module is a stack of multiple layers i.e. superstrate (glass), solar cell assembly sandwiched between two layers of the polymeric encapsulant and the substrate (backsheet/glass). Typically, the most common architecture used in glass/backsheet (G/B) is demonstrated in Fig. 1 (a). However, with the inception of new module technologies (e.g. bifacial) and the advantage of the moisture barrier layer at the rear side of the module, glass/glass (G/G) configuration (shown in Fig. 1 (b)) is poised to be emerging [2].

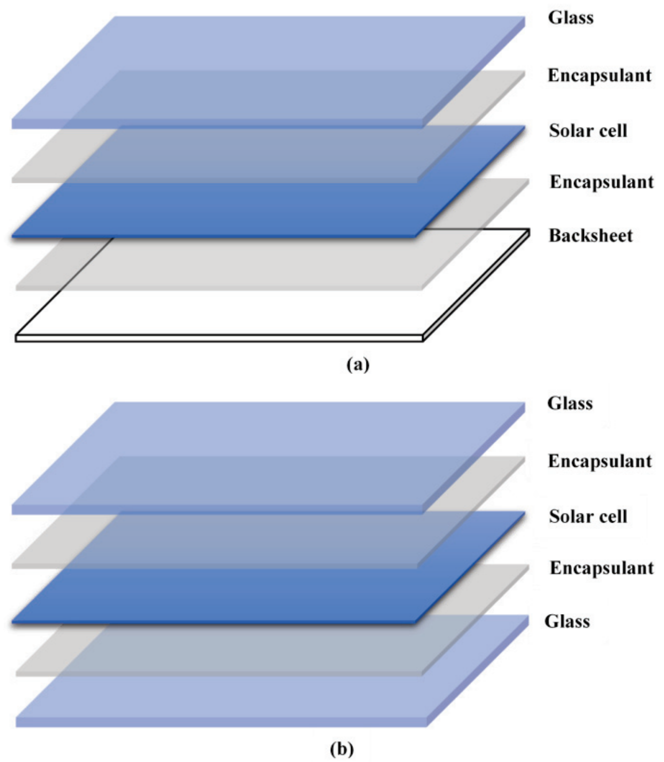

Fig. 1: Schematic diagram of a c-Si PV module (a) Glass/Backsheet module (b) Glass/Glass module

Encapsulant is an important constituent of the module laminate, which provides the structural support, good optical coupling between superstrate/cell and cell/substrate interfaces, high thermal conduction and electrical isolation. In the past 35 years, ethylene vinyl acetate (EVA) has been a preferred choice for PV encapsulant due to field-demonstrated thermal stability and low cost. It is a semi-crystalline random copolymer synthesized from polyethylene (crystalline) and vinyl acetate (VA) (amorphous). To increase the stability and durability of EVA against environmental factors, certain additives are added such as Cyasorb UV 531 (UV absorber), Lupersol 101 (curing agent), Naugard P (anti-oxidant/hydroperoxide decomposer)

This paper was submitted on 23rd August 2019. This work was partly supported by the U.S. Department of Energy under award DE-EE0008565.

A. Patel, A. Sinha, and G. Tamizhmani are affiliated with the Photovoltaic Reliability Laboratory, Arizona State University, Mesa, AZ 85212 USA (e-mail: manit@asu.edu). The authors would like to acknowledge Dr. Akash Kumar for his technical contribution.

Digital Object Identifier 10.1109/JPHOTOV.2019.2958516

Table I: List of unexposed and exposed EVA samples to be tested

Extracted EVA samples	EVA sample type	Sample source
Unexposed	Uncured	Fresh EVA roll
	Cured	From a freshly laminated module
Field-exposed	Cell center	From field-retrieved modules: type I (glass/backsheet with no cracked cells), type II (glass/backsheet with multiple cracked cells), and type III (glass/glass with no cracked cells)
	Cell edge	
	Non-cell area	

and Tinuvin 770 (UV stabilizer) [3], [4].

Under field conditions, EVA aging occurs via two main degradation modes: delamination and discoloration. Delamination is caused by the breaking of interfacial bonds between the encapsulant and adjacent layers in humid environment [5]. Discoloration is attributed to the depletion of additives and/or occurrence of Norrish reactions under prolonged exposure to UV light and high operating temperature [3], [4], [6]–[8].

There are two possible mechanisms for EVA discoloration. The highly favored mechanism is the decomposition of additives in EVA due to high operating temperature and UV exposure [4]. Decomposition of Cyasorb (UV absorber) under photolysis leads to interactions between the crosslinking peroxide agent and stabilizers resulting in the EVA degradation problem.

The other EVA discoloration mechanism often cited in the literature is through polyene formation by Norrish reactions [3]. The onset of EVA degradation process occurs with the chain scission and an increase in crosslinking in EVA due to UV irradiation. Both processes occur in vinyl acetate groups because the photostability of polyethylene is higher than vinyl acetate [3]. The depletion of stabilizers in the EVA encapsulant due to the action of UV and heat increases crosslinking in EVA and accelerates the formation of polyenes and volatile acetic acid by Norrish II reaction [3], [9]. An increase in crosslinking from 70% to greater than 90% has been reported in discolored regions of EVA [3]. As reported by Oliveira and Pern [10], [3], polyenes containing unsaturated chromophores $[C{=}C]_n$ cause EVA browning. Hence, longer the chain of polyenes, higher will be the EVA discoloration. Longer polyenic chromophores can be detected by FTIR-ATR in the 1500-1650 cm^{-1} region [6]. Acetic acid produced by the Norrish II reaction acts as a self-catalyst and accelerates the EVA degradation.

Photobleaching is a competing reaction that occurs in the presence of oxygen. Oxidation reduces the length of polyenes and eliminates discoloration, eventually lowering the degradation rate [3]. The shortening of polyenes turns the dark brown color of EVA encapsulant into light yellow/white (translucent). The diffusion of oxygen/air into EVA is a prerequisite for the occurrence of photobleaching, which takes place even at room temperature [3].

Several studies have been published on the analysis of EVA degradation in G/B modules using chemical characterization techniques [11]–[17]. Like G/B modules, the G/G modules are also seen to be affected by similar encapsulant degradation modes [18]. However, the presence of an impermeable rear glass layer restricts the photobleaching action of discolored EVA. Hence the underlying degradation mechanism pathway would be expected to be different in both architecture types. There is very limited literature on field studies about the EVA degradation in G/G modules. The objective of this paper is to compare EVA encapsulant degradation in G/B and G/G field-aged c-Si PV modules and understand the underlying mechanisms by correlating the changes in EVA properties and module electrical performance.

II. Methodology

A. Test modules and sample preparation

Test modules are listed in Table I. Three fielded crystalline-silicon (c-Si) modules of different module manufacturers, architecture, and exposure periods with EVA encapsulant were considered for this study. These modules were aged under a hot and dry climate of Arizona (AZ). Among them, two were glass/backsheet modules and labeled as modules type I and type II that were exposed for 18 years and 21 years, respectively, while module type III was a 10-year-old glass/glass module. Each module was first characterized by a suite of non-destructive methods to obtain the health report of electrical performance before it was diced to extract the degraded EVA from different regions. The harvested piece of front EVA was analyzed with a set of destructive analytical methods to determine the changes in encapsulant properties. The results were compared against the pristine EVA extracted from the unexposed module and uncured EVA taken from a fresh roll.

The browned cells of interest were identified in all three field-aged modules from the UVF images. These cells were cut using a diamond tip Dremel tool. The front EVA was extracted by peeling off the backsheet and back EVA layers with a scalpel. A small section of EVA from the cell center, cell edge, and non-cell region was cut, wrapped in aluminum foil, and stored in an air-tight plastic bag to prevent them from contamination and environmental exposure. 7,6, and 4 cells were cut from modules type I, II, and III respectively. A summary of EVA samples that were tested is provided in Table I. All the EVA samples from the modules under consideration including the unexposed EVA were manufactured by Specialized Technology Resources, Inc. formerly known as Springborn Laboratories.

B. Module and EVA Characterization Methods

The test samples were characterized by a suite of non-destructive as well as destructive methods, which are described in this section.

1) Visual Inspection and Ultra-violet Fluorescence Imaging

The modules were examined visually under high illumination (1000 lux) as defined by IEC 61215 standard, to determine any traces of discoloration and other physical changes in different parts of the laminate.

A non-destructive, fast, and contactless method of UVF imaging was employed to detect EVA discoloration. The experimental setup is a custom-designed UV illumination system comprising of two arrays of 15 UV lamps each inclined at an angle of 45° w.r.t. the module surface to eliminate the glare in the images from the reflection of incident UV light. The module was illuminated by the UV light (wavelength 385-395 nm) and the emitted fluorescence from degraded EVA was captured by a digital visual camera. These UVF images served as a reference to select the regions of interest for extracting the EVA samples.

2) I-V Measurement

The *I-V* measurements were taken to calculate I_{sc} and P_{max} degradation rates that can be linked to changes in EVA material properties. The module-level *I-V* data were collected outdoors using a daystar *I-V* curve tracer. The modules were cooled to about 15°C and then placed on a two-axis tracker at zero angle of incidence. With the increase in module temperature, multiple curves were taken at regular intervals. A calibrated reference cell was mounted in the same plane of array as the test modules. To measure the module temperature, a K-type thermocouple (accuracy ±1°C) was attached to the rear side of the module. The readings were recorded using an *I-V* PC software and then translated to the STC conditions (25°C, 1000W/m^2) using the interpolation method [19]. I_{sc} is directly proportional to the number of photons that are incident on the cell and is a measure of transmission loss due to EVA browning. Using the *I-V* data and field-exposure time, I_{sc} and P_{max} degradation rates were calculated from equations (1) and (2) respectively as given below:

$$I_{sc}\ deg\ rate\ (\%/year) = \frac{\frac{I_{sc,0} - I_{sc,t}}{I_{sc,0}} \times 100}{years\ of\ field\ exposure} \tag{1}$$

$$P_{max}\ deg\ rate\ (\%/year) = \frac{\frac{P_{\max,0} - P_{max,t}}{P_{max,0}} \times 100}{years\ of\ field\ exposure} \tag{2}$$

where the states 0 and t designate to the pre and post-exposure time.

3) Colorimetry

Colorimetry was performed on extracted EVA to quantify the color change in the polymeric encapsulant material through a metric known as yellowness index (YI) [20]. The YI readings were recorded using an Xrite Ci-60 spectrophotometer. The instrument was calibrated using a black and a white reference. Higher YI value corresponds to the darker color shade, which indicates greater extent of EVA degradation.

4) Differential Scanning Calorimetry

DSC method is used to analyze the phase behavior of the EVA samples and calculate the degree of crystallinity with the help of the total enthalpy equation expressed in (3) [21], [22]:

$$\chi_c = \frac{\Delta H_m}{\Delta H_{100}} \times 100 \tag{3}$$

where
χ_c = degree of crystallinity (%)
ΔH_m = specific enthalpy of melting of a test sample (J/g)
ΔH_{100} = specific enthalpy of melting for 100% crystalline polyethylene (293 J/g) [23]

The EVA samples were placed in the hermetically sealed aluminum pans. A heat-cool-heat cycle was run in a nitrogen atmosphere with a constant flow rate of 50 ml/min. The DSC data were collected using the DSC instrument Q20 manufactured by TA Instruments. The instrument was calibrated with a reference indium material. The thermal process sequence of the heat-cool-heat cycle is given below [24]:

i. Ramp up from ambient temperature (25ºC) to 200ºC at a heating rate of 10ºC/min
ii. Ramp down from 200ºC to -50ºC at a cooling rate of 10ºC/min
iii. Ramp up from -50ºC to 200ºC at a heating rate of 10ºC/min

5) Thermogravimetric Analysis

TGA method is utilized to determine the thermal stability of EVA. The sample is heated and the change in its weight was recorded as a function of temperature. The first step in the TGA weight loss curve corresponds to the loss of volatile acetic acid content (%) that provides the estimation of vinyl acetate (VA) content using equation (4) [12][25]:

$$VA\ content(\%) = HAc\ content\ (\%) \times \frac{MW_{(VA)}}{MW_{(HAc)}} \tag{4}$$

where
HAc = Acetic acid
$MW_{(VA)}$= Molecular weight of VA (86.1 g/mol)
$MW_{(HAc)}$= Molecular weight of acetic acid (60.1 g/mol)

Upon EVA degradation, acetic acid is a major by-product derived from VA group during Norrish II reaction. Acetic acid acts as a self-catalyst and further accelerates EVA degradation. Hence, HAc content obtained from the TGA curves would be a good indication of VA content present in EVA.

EVA samples were placed in open aluminum pans and the temperature was raised from room temperature to 500 ºC at the rate of 15ºC/min. The measurements were done in nitrogen ambient purged at the flow rate of 60 ml/min. The TGA data were collected using Q50 TGA equipment manufactured by TA Instruments.

6) Raman Spectroscopy

Raman spectroscopy determines the changes in molecular vibrations and fluorescence background in degraded EVA [26]. During the process of crosslinking, the terminal -CH_3 groups of the VA group take part in radical reactions wherein -CH_3 groups are converted into CH_2 bridges [27]. This utilizes the Raman spectra data to calculate the degree of crosslinking (or gel content) using equation (5) [27], [28]:

$$Crosslinking\ ratio = \frac{2941\ cm^{-1}}{2891 cm^{-1}} \quad (5)$$

where 2941 cm^{-1} and 2891 cm^{-1} correspond to CH_2 and CH_3 symmetric stretching, respectively.

The spectra were collected using an Acton 300i spectrograph in a 180º geometry and a back-thinned Princeton Instruments liquid nitrogen cooled CCD detector. The sample was excited by a 150 mW Coherent Sapphire SF laser with a 532 nm laser wavelength. The laser was focused onto the sample using a 50X super long working distance plan APO Mitutoyo objective with a numerical aperture of 0.42. The spectrometer was calibrated using the cyclohexane spectrum as a reference. The data were further processed in Spectragryph software.

7) Fourier Transform Infrared Spectroscopy

FTIR method was utilized to identify the presence of functional groups of EVA degradation products caused by photochemical reactions.

EVA is too thick for FTIR investigation to be performed in transmission mode. In this mode, the thick sample generates noisy peaks by absorbing all the radiation before passing it through the sample for detection. Hence, to obtain distinguishable peaks in the FTIR spectrum, Attenuated Total Reflectance (ATR) approach was employed and the data were collected using the 4300 Agilent handheld FTIR. Unlike FTIR which works on the transmission mode, ATR-FTIR works on the principle of total internal reflection [29], [30]. The sample was placed in contact with the ATR crystal (here, diamond) tip probe to get the FTIR spectrum. The output spectrum is in the mid-IR (2.5-25 µm) wavelength range (wavenumbers 4000-400 cm^{-1}).

III. Results and Discussion

A. Discoloration area from visual and UVF images

Fig. 2 shows the juxtaposed images from visual inspection and UVF imaging of modules type I, II and III. The images of modules type I and II exhibit prominent encapsulant browning over the central regions of the cells. However, the cell edges and non-cell regions are light yellow indicating photobleaching action through the breathable backsheet. On the other hand, module type III shows intense brown discoloration of EVA over the entire module including cell centers, edges, and non-cell regions. The presence of impermeable glass in G/G modules restricts oxygen ingression inside the module, resulting in no photobleaching.

The UVF images reveal that type I module exhibited nearly uniform browning at the cell centers whereas type II showed few cells with skewed patterns of browning at the centers. This difference can be attributed to cell microcracks in module type II, which opened the pathways for oxygen ingression causing enhanced photobleaching. Through image processing of scanning electron microscope images of cells, it was also found that the cells used in type II (200 µm thick) were thinner than type I (300 µm thick), and hence more susceptible to cracking under the field stresses.

B. Estimation of degradation rates from I-V measurement

Encapsulant degradation has an adverse impact on material transparency that directly reduces light transmission to the solar cells. Consequently, the photon to electron conversion efficiency declines, resulting in a drop in I_{sc} and P_{max}. The I_{sc} and P_{max} degradation rates of test modules were calculated based on their nameplate ratings and presented in Table II. The degradation rates (I_{sc}, P_{max}) are considerably higher for G/G module type III (1.46, 2.28) as compared to G/B modules type I (0.41, 1.01) and type II (0.29, 0.44). A greater extent of EVA degradation in G/G configured modules as compared to G/B modules is attributed to photobleaching around the cell edges, which is also evident from visual inspection and UVF imaging results. Hence, photobleaching in G/B modules lowers the encapsulant degradation rate by partially increasing the optical transparency i.e. changing browned EVA to light yellow which

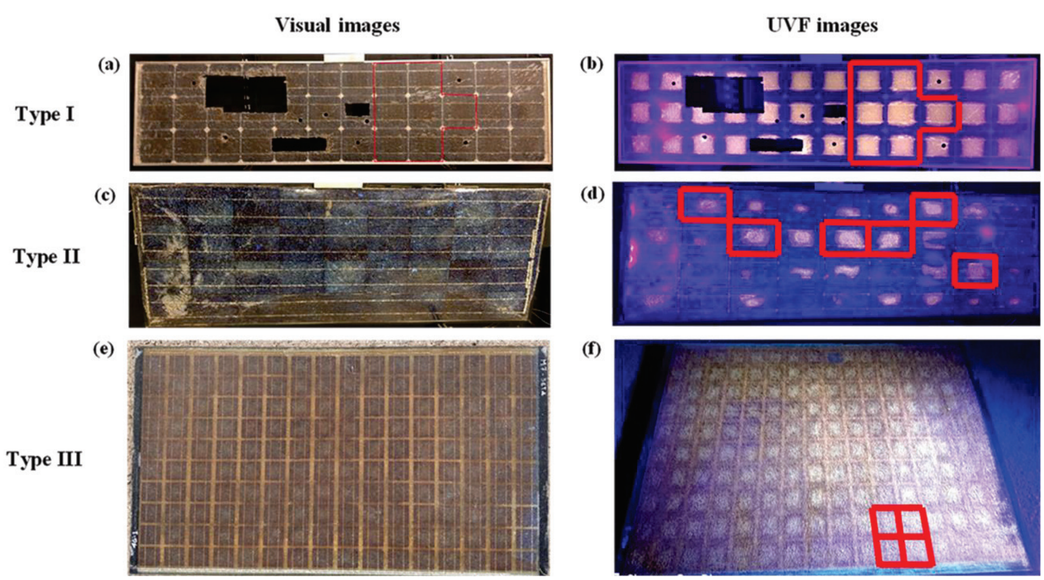

Fig. 2: Visual and UVF images of module type I (a-b), module type II (c-d), and module type III (e-f). EVA samples were extracted from cells marked in red in UVF images. The hollow space in visual and UVF images of module type I correspond to the cells extracted for a different purpose

Table II: Calculation of I_{sc} and P_{max} degradation rates per year for modules type I, type II, and type III

I_{sc} and P_{max} degradation rates						
	Module type I (Glass/Backsheet with no cracked cells)		Module type II (Glass/Backsheet with multiple cracked cells)		Module type III (Glass/Glass with no cracked cells)	
	I_{sc}	P_{max}	I_{sc}	P_{max}	I_{sc}	P_{max}
Pre-exposure (nameplate) reading	3.35 A	53.00 W	3.89 A	62.50 W	4.95 A	300.00 W
Post-exposure reading	3.10 A	43.40 W	3.65 A	56.70 W	4.23 A	231.60 W
Degradation (%)	7.46	18.11	6.17	9.28	14.54	22.80
Years of field exposure	18		21		10	
Degradation rate (%/year)	0.41	1.01	0.29	0.44	1.46	2.28

in turn restricts the degradation rate. It has been observed that the contribution of I_{sc} loss to P_{max} loss is significantly high. I_{sc} loss accounts for 45% and 65% of P_{max} drop in G/B and G/G modules respectively.

C. *Quantification of Encapsulant Browning from Colorimetry*

Fig. 3 reports YI values for unexposed EVA and field-aged samples from modules type I, II and III.

Uncured and cured EVA (i.e. unexposed EVA) recorded YI of 7.5 and 8.7, respectively, while degraded EVA samples from all three modules produced significantly high YI. Higher YI value indicates intense EVA browning. Among the degraded EVA samples, a clear trend is observed i.e. module type III has the highest YI values, followed by modules type I and type II. The non-cell region in module type III showed the highest YI values, followed by cell edges and then cell centers. Due to the presence of an impervious glass layer at the rear side, the acetic acid and other volatile degradation products get entrapped within the module and accelerate the degradation reaction. Non-cell EVA is double layered consisting of fused front and back EVA sheets. This results in greater amount of acetic acid production causing higher discoloration in that region. High cell temperature at the center will favor the diffusion of acetic acid from the cell region to the non-cell region where it accumulates and causes yellowing to intensify to dark brown.

In contrast, for modules type I and II, cell centers showed the highest YI values and longer oxygen diffusion lengths. Interestingly, in module type I, cell edges showed higher YI values than non-cell region. The increased photobleaching over time due to cell cracks in module type II altered the YI trend for G/B modules.

Moreover, the backsheet helps in diffusing out the acetic acid produced and thereby, prevents additional catalytic degradation caused by acetic acid.

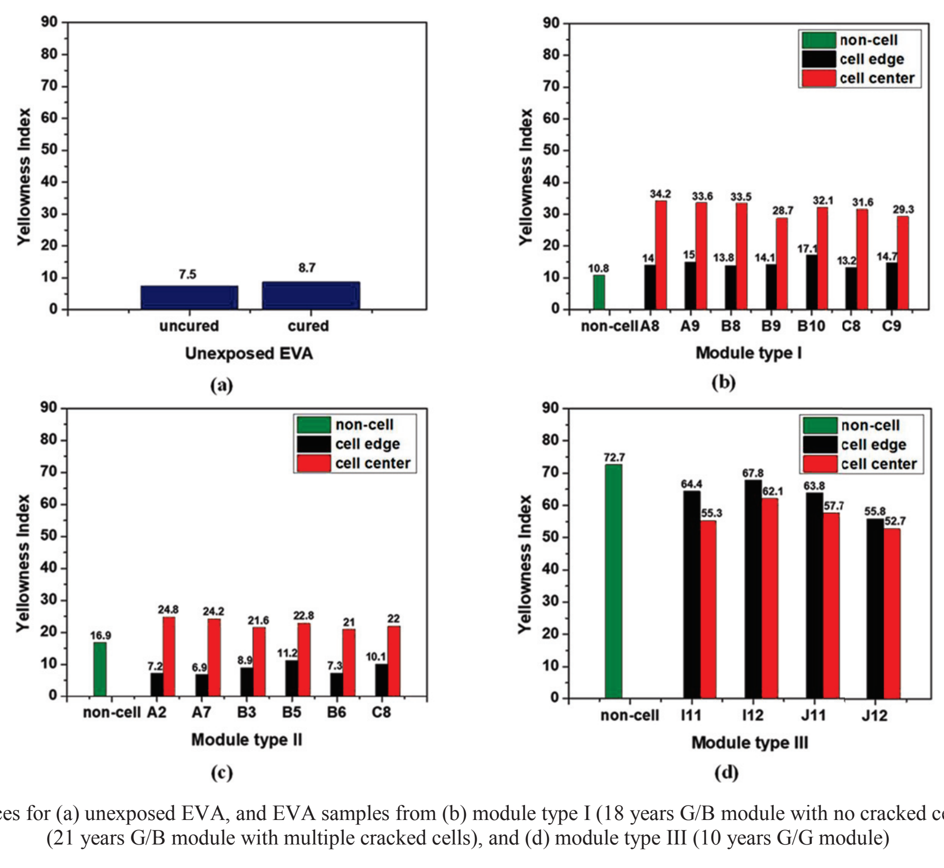

Fig. 3: Yellowness indices for (a) unexposed EVA, and EVA samples from (b) module type I (18 years G/B module with no cracked cells), (c) module type II (21 years G/B module with multiple cracked cells), and (d) module type III (10 years G/G module)

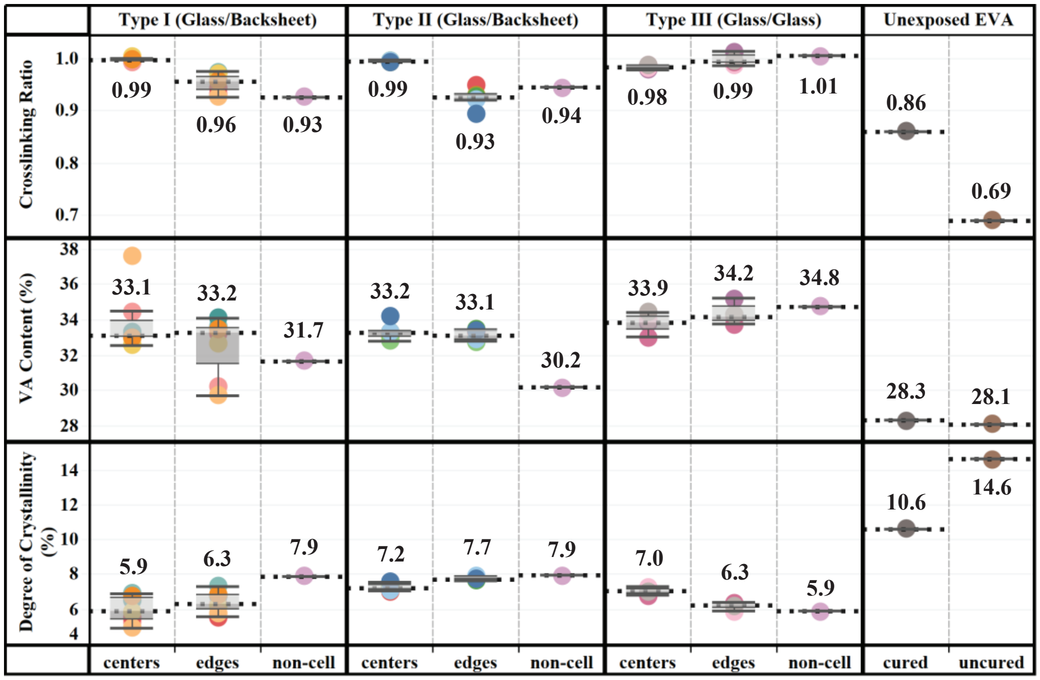

Fig. 4: Graphical representation of the degree of crystallinity (%), VA content (%), and crosslinking ratio for degraded EVA samples from modules type I, type II, and type III, and unexposed EVA (uncured and cured)

D. Determination of Degree of Crystallinity from DSC

Fig. 4 illustrates degree of crystallinity of different EVA samples. Degraded EVA samples from both module configurations gave an overall lower degree of crystallinity than unexposed EVA. Uncured and cured EVA had degree of crystallinity of 14.6% and 10.6%, respectively.

In modules type I and II, degree of crystallinity is the highest in non-cell regions and the lowest in cell centers. However, the trend is reversed for module type III. The reason could be deformation of the original EVA structure by UV rays and high field temperature. The VA group in EVA perturbs the ordered crystal packing of long chains of polyethylene (PE) by taking part in several chemical reactions, thus bringing complexity in the polymer. The field exposure alters the EVA structure by decreasing the molecular weight of EVA i.e. breaking the longer crystalline PE sequences and leaving behind non-crystallite structures. This decreases the degree of crystallinity in EVA post-field exposure. Hence, lower the degree of crystallinity, higher would be the EVA degradation. Another reason for the reversal of the crystallinity trend in module type III is the acetic acid entrapment. It acts as an auto-catalyst and further accelerates EVA degradation. Since EVA thickness in the non-cell region is twice the cell region, the production of acetic acid will be higher, particularly in the absence of photobleaching. It leads to a higher decrease in crystallinity in that region.

E. Calculation of VA content from TGA

The VA content (%) determined from TGA for various EVA samples is shown in Fig. 4. Uncured and cured EVA contain 28.1% and 28.3% VA content, respectively. However, EVA samples from degraded modules showed overall higher VA content than unaged EVA. This infers that higher VA content corresponds to higher EVA degradation.

The EVA samples from G/B modules exhibited higher VA content in cell centers than in non-cell regions. This small dissimilarity in the VA trend for G/B modules is attributed to non-uniform browning caused by the cell cracks and increased photobleaching in type II module. However, module type III follows the opposite trend depicting the highest VA content in non-cell regions and the lowest in cell centers. The VA content trend reversal between G/B and G/G modules is the result of the changes in crystallinity and increased amorphization in EVA favored by a decrease in the crystalline constraints of PE on amorphous parts of EVA due to major structural distortion and formation of disorganized crystals. Increased VA content enhances the deacetylation rate causing higher acetic acid production and significant EVA browning. This is in close agreement with the YI and crystallinity results in previous sections. Therefore, higher the VA content, higher would be EVA degradation.

F. Estimation of Crosslinking Ratio from Raman Spectra

Fig. 4 details the variation of crosslinking ratio for EVA samples obtained from Raman spectra. The measured crosslinking is 69% and 86% in uncured and cured EVA respectively, which according to the literature is deemed sufficient after lamination [27]. However, degraded EVA samples from all three modules showed greater than 90% degree of crosslinking. This demonstrates that higher degree of crosslinking is linked to greater degradation of EVA material.

EVA from G/B modules showed higher degree of crosslinking in cell centers and lower in the inter-cell regions. A slightly contrasting trend in G/B modules can be attributed to the presence of several cell microcracks in module type II which encouraged further photobleaching over time. Further, EVA in G/G module has the highest crosslinking in non-cell regions among all the cases. Crosslinking or branching interferes with

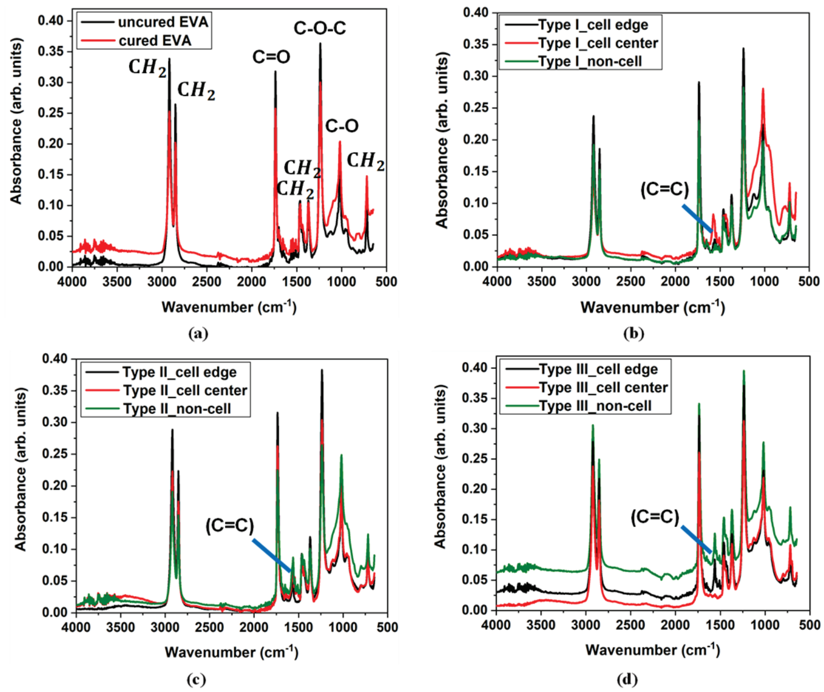

Fig. 5: FTIR spectra for unexposed EVA and degraded EVA samples (non-cell region, cell centers and cell edges) from modules type I, type II, and type III

the orderly chain packing of the molecules in the EVA polymer. Hence, it reduces the crystallinity of the polymer and increases its VA content which aligns with the results from the above-mentioned techniques. An increase in VA content increases the rate of deacetylation reaction, thereby increasing the production of acetic acid and polyenes. There is a possibility that the EVA thickness, the spacing of the cells and the absence of oxygen (which could have further increased crosslinking) can also be some of the factors leading to the change in the order of degree of crosslinking between G/B and G/G modules.

G. *Presence of degradation products*

The FTIR spectra of the unexposed and selected degraded EVA samples are shown in Fig. 5. The FTIR spectra for unexposed EVA consist of peaks corresponding to PE and VA. The PE peaks are at 720 cm^{-1} (CH_2 vibration of the ethylene backbone), 1461 cm^{-1} (CH_2 bending), 2850 cm^{-1} (CH_2 symmetric stretching), and 2918 cm^{-1} (CH_2 asymmetric stretching). The VA peaks lie at 1018 cm^{-1} (C-O stretching), 1237 cm^{-1} (C-O-C stretching), 1371 cm^{-1} (CH_2 bending in VA group), and 1736 cm^{-1} (C=O stretching), respectively. Degraded EVA samples from G/B and G/G modules indicated polyenic production (C=C) with conspicuous peaks at about 1560 cm^{-1} in addition to the characteristic EVA peaks. These results corroborate the polyene formation through Norrish II reaction. However, the polyene absorption in FTIR spectra is different between G/B and G/G modules. G/B modules (type I and II) have more intense polyene absorption in cell centers than in cell edges and non-cell regions whereas, in G/G module, the non-cell region has more intense polyene absorption than cell centers and edges. The degradation products derived from the decomposition of additives tend to remain below the FTIR detection level. This necessitates relying on other analytical techniques such as mass spectrometry with higher sensitivity to detect additives that are not detectable by FTIR.

H. *Correlation between different characterization methods*

From the previous sections, valuable information about EVA material properties from aging has been extracted. Correlations were established to understand the effects of EVA degradation on its physical and chemical properties as well as on the electrical performance of the module laminate. The average values of the material properties measured at cell edges and cell centers in each module type were considered.

Fig. 6 illustrates the relationship established between the crosslinking ratio, degree of crystallinity, and YI of EVA encapsulant as a function of VA content. YI of EVA is directly related to its VA content. Therefore, degraded EVA follows a common trend irrespective of module construction i.e. an increase in the crosslinking, VA content and YI along with a decrease in the degree of crystallinity.

Another observation is that crosslinking, and crystallinity have an inverse relationship. This is clearly because crosslinking caused by UV rays and temperature interferes with the molecular packing of atoms in PE molecule of EVA and reduces its molecular weight. Besides, the VA group too interferes with the stereoregularity of PE molecules which reduces the degree of crystallinity.

Table *III* relates the module performance losses (I_{sc} and P_{max}) to the changes in YI of extracted EVA properties upon degradation. Average values of YI calculated for cell center EVA are taken into consideration. Higher browning causes transmission losses which reduce the electrical performance of the modules. Hence, the module I_{sc} degradation rate is linearly proportional to the YI of EVA. YI along with I_{sc} degradation rate for the G/G module is higher than that of G/B modules. Despite being field-aged for a longer period, module type II has lower YI and degradation rates. This can be attributed to the

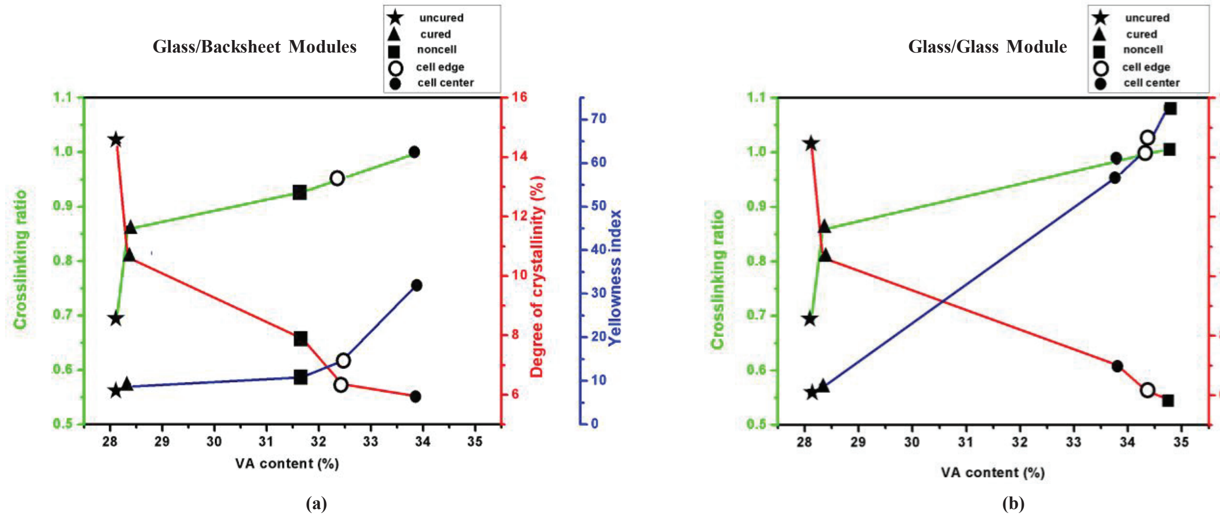

Fig. 6: Correlation between crosslinking ratio, VA content, degree of crystallinity, and YI for (a) glass/backsheet, and (b) glass/glass module, respectively

Table III: Correlation between YI with I_{sc}, and P_{max} for modules type I, type II, and type III

	Field-aged Modules		
Modules	Type I	Type II	Type III
YI (centers_avg)	32.13	22.38	56.50
I_{sc} degradation rate (%/year)	0.41	0.29	1.46
P_{max} degradation rate (%/year)	1.01	0.44	2.28

presence of cell cracks that promoted photobleaching and recovery of transmission loss from browning. Since I_{sc} is one of the factors contributing to P_{max}, P_{max} also decreases with an increase in browning.

IV. Conclusions

A comprehensive investigation of EVA encapsulant degradation in two different module constructions-glass/backsheet (type I and II) and glass/glass (type III) field-aged c-Si PV modules has been presented. Module and material level characterization techniques were performed to establish correlations between EVA properties, module performance, and degradation extent. In contrast to unexposed EVA, highly browned EVA showed significant increase in the degree of crosslinking, VA content, YI and polyene formation with reduction in crystallinity. At module level, EVA browning caused higher I_{sc} and P_{max} losses. In modules type I, II, and III, the average degree of crystallinity for cell center EVA is 5.9%, 7.2%, and 7.0%, respectively whereas for non-cell EVA is 7.9%, 7.9%, and 5.9%, respectively. Similarly, the average VA content and crosslinking ratio for cell center EVA in modules type I, II, and III are 33.1%, 33.2%, and 33.9% and 0.99, 0.99, and 0.98, respectively whereas for non-cell EVA is 31.7%, 30.2%, and 34.8% and 0.93, 0.94, and 1.0, respectively. The uncertainties in the results for type II module have been attributed to non-uniform browning caused by increased photobleaching through cell cracks. Despite being exposed to UV light for a reduced period, G/G module shows higher EVA discoloration and thereby higher performance losses than G/B module. The information obtained on the discoloration effects on the physical/structural/chemical properties of EVA is consistent with the module *I-V* measurements. I_{sc} loss accounts for about 45% and 65% of P_{max} loss in G/B and G/G modules, respectively. It can be inferred that EVA browning has been a major cause of performance degradation in field-aged modules.

The absence of polymeric breathable backsheet and thereby photobleaching, and entrapment of acetic acid and other volatile degradation products in EVA encapsulant in G/G modules seems to play a major role in the difference in EVA degradation pathway between two module configurations. Hence, it can be concluded that EVA might have been a good choice of an encapsulant for G/B modules over the years but may not be an appropriate choice for G/G modules. Ionomers or polyester-based encapsulants like polyolefins (POE) could be best suited for G/G modules.

References

[1] A. Perea, C. Smith, M. Davis, A. Mond, B. Gallagher, S. Rumery, A. Holm, R. Goldstein, and J. Baca, "U.S. Solar Market Insight Executive Summary-2018 year in review," 2019.

[2] G. Cattaneo, A. Faes, H. Li, F. Galliano, M. Gragert, Y. Yao, R. Grischke, T. Söderström, M. Despeisse, C. Ballif, and L. Perret-Aebi, "Lamination process and encapsulation materials for glass-glass PV module design," *Photovoltaics Int.*, pp. 1–8, 2015.

[3] A. W. Czanderna and F. J. Pern, "Encapsulation of PV modules using ethylene vinyl acetate copolymer as a pottant: A critical review," *Sol. Energy Mater. Sol. Cells*, vol. 43, no. 2, pp. 101–181, 1996.

[4] P. Klemchuk, M. Ezrin, G. Lavigne, W. Holley, J. Galica, and S. Agro, "Investigation of the degradation and stabilization of EVA-based encapsulant in field-aged solar energy modules," *Polym. Degrad. Stab.*, vol. 55, no. 3, pp. 347–365, 1997.

[5] D. Wu, Z. Jiang, T. R. Betts, and R. Gottschalg, "Degradation of interfacial adhesion strength within photovoltaic mini-modules during damp-heat exposure," *Prog. Photovoltaics Res. Appl.*, vol. 22, pp. 796–809, 2014.

[6] F. J. Pern, “Factors that affect the EVA encapsulant discoloration rate upon accelerated exposure,” *Sol. Energy Mater. Sol. Cells*, vol. 41–42, pp. 587–615, 1996.
[7] F. J. Pern and A. W. Czanderna, “EVA degradation mechanisms simulating those in PV modules,” vol. 268, pp. 445–452, 2008.
[8] M. Bregulla, M. Köhl, B. Lampe, G. Oreski, D. Philipp, G. Wallner, and K. Weiß, “Degradation Mechanisms of Ethylene-Vinyl-Acetate Copolymer–New Studies Including Ultra Fast Cure Foils,” in *22nd European Photovoltaic Solar Energy Conference*, 2007, pp. 5–8.
[9] F. J. Pern and A. W. Czanderna, “Characterization of ethylene vinyl acetate (EVA) encapsulant: Effects of thermal processing and weathering degradation on its discoloration,” *Sol. Energy Mater. Sol. Cells*, vol. 25, no. 1–2, pp. 3–23, 1992.
[10] M. C. C. de Oliveira, A. S. A. Diniz Cardoso, M. M. Viana, and V. de F. C. Lins, “The causes and effects of degradation of encapsulant ethylene vinyl acetate copolymer (EVA) in crystalline silicon photovoltaic modules: A review,” *Renew. Sustain. Energy Rev.*, vol. 81, pp. 2299–2317, 2017.
[11] K. Agroui and G. Collins, “Thermal relaxations and transitions in EVA encapsulant material during photovoltaic module encapsulation process,” *Mater. Process. energy Commun. Curr. Res. Technol. Dev.*, pp. 150–157, 2013.
[12] R. Polanský, M. Pinkerová, M. Bartůňková, and P. Prosr, “Mechanical behavior and thermal stability of eva encapsulant material used in photovoltaic modules,” *J. Electr. Eng.*, vol. 64, no. 6, pp. 361–365, 2013.
[13] C. Peike, T. Kaltenbach, K.-A. Weiss, and M. Koehl, “Non-destructive degradation analysis of encapsulants in PV modules by Raman Spectroscopy,” *Sol. Energy Mater. Sol. Cells*, vol. 95, no. 7, pp. 1686–1693, 2011.
[14] C. Peike, W. Phondongnok, T. Kaltenbach, K.-A. Weiss, and M. Koehl, “Non-destructive determination of the cross-linking degree of EVA by Raman Spectroscopy,” *Open J. Renew. Energy Sustain. Dev.*, vol. 1, no. 1, pp. 14–21, 2014.
[15] E. Planes, B. Yrieix, C. Bas, and L. Flandin, “Chemical degradation of the encapsulation system in flexible PV panel as revealed by infrared and Raman microscopies,” *Sol. Energy Mater. Sol. Cells*, vol. 122, pp. 15–23, 2013.
[16] F. J. Pern, “Ethylene-Vinyl Acetate (EVA) Encapsulants for Photovoltaic Modules: Degradation and Discoloration Mechanisms and Formulation Modifications for Improved Photostability,” *Macromol. Mater. Eng.*, vol. 252, no. 1, pp. 195–216, 1997.
[17] K. Dolia, “Accelerated UV Testing and Characterization of PV Modules with UV-cut and UV-pass EVA Encapsulants,” M.S. Thesis, Arizona State University, 2018.
[18] A. Skoczek, T. Sample, and E. D. Dunlop, “The Results of Performance Measurements of Field-aged Crystalline Silicon Photovoltaic Modules,” *Prog. Photovoltaics Res. Appl.*, vol. 17, pp. 227–240, 2008.
[19] G. Tamizhmani, K. Paghasian, J. Kuitche, M. G. Vemula, and G. Sivasubramanian, “Photovoltaic Module Power Rating per IEC 61853-1 Standard: A Study Under Natural Sunlight,” 2011.
[20] “ASTM E313-15e1, Standard Practice for Calculating Yellowness and Whiteness Indices from Instrumentally Measured Color Coordinates,” ASTM International, West Conshohocken, PA, 2015, www.astm.org
[21] X. M. Shi, J. Zhang, J. Jin, and S. J. Chen, “Non-isothermal crystallization and melting of ethylene-vinyl acetate copolymers with different vinyl acetate contents,” *Express Polym. Lett.*, vol. 2, no. 9, pp. 623–629, 2008.
[22] S. Bistac, P. Kunemann, and J. Schultz, “Crystalline modifications of ethylene-vinyl acetate copolymers induced by a tensile drawing: effect of the molecular weight,” *Polymer (Guildf).*, vol. 39, no. 20, pp. 4875–4881, 1998.
[23] C. C. Ibeh, “Crystallinity and Crystallization in Polymers and Plastics,” in *Thermoplastic Materials: Properties, Manufacturing Methods, and Applications*, 1st ed., CRC Press, 2011, p. 640.
[24] M. Chicca, “Characterization and Analysis of Long Term Field Aged Photovoltaic Modules and Encapsulant Materials,” M.S. Thesis, Arizona State University, 2015.
[25] C. Potter, S. Cotts, and F. Wiebke, “Materials Characterization by Thermal Analysis (DSC & TGA), Rheology, and Dynamic Mechanical Analysis Facts about TA Instruments.”
[26] C. Hirschl, M. DeBiasio, L. Neumaier, R. Leitner, G. Eder, S. Seufzer, and M. Kraft, “In-line Raman Analysis of Ethylene Vinyl Acetate Curing for and in Industrial PV Module Manufacturing,” in *International Conference on Advanced Vibrational Spectroscopy 2015 (ICAVS-8), Project: EVAnetz*, 2015.
[27] C. Hirschl, M. Biebl-Rydlo, M. DeBiasio, W. Muhleisen, L. Neumaier, W. Scherf, G. Oreski, G. Eder, B. Chernev, W. Schwab, and M. Kraft, “Determining the degree of crosslinking of ethylene vinyl acetate photovoltaic module encapsulants-A comparative study,” *Sol. Energy Mater. Sol. Cells*, vol. 116, pp. 203–218, 2013.
[28] B. S. Chernev, C. Hirschl, and G. C. Eder, “Non-Destructive Determination of Ethylene Vinyl Acetate Cross-Linking in Photovoltaic (PV) Modules by Raman Spectroscopy,” *Appl. Spectrosc.*, vol. 67, no. 11, pp. 1296–1301, 2013.
[29] D. Wu, “Investigation of the reliability of the encapsulation system of photovoltaic modules,” Ph.D. dissertation, Loughborough University, 2015.
[30] R. P. D’Amelia, S. Gentile, W. F. Nirode, and L. Huang, “Quantitative Analysis of Copolymers and Blends of Polyvinyl Acetate (PVAc) Using Fourier Transform Infrared Spectroscopy (FTIR) and Elemental Analysis (EA),” *World J. Chem. Educ.*, vol. 4, no. 2, pp. 25–31, 2016.